Nuclear Science and Techniques (2025) 36:128
https://doi.org/10.1007/s41365-025-01737-w

On shape coexistence and possible shape isomers of nuclei around ^{172}Hg

Xin Guan[1] · Jing Guo[1] · Qi-Wen Sun[1] · Bożena Nerlo-Pomorska[2] · Krzysztof Pomorski[3]

Received: 9 January 2025 / Revised: 1 February 2025 / Accepted: 6 February 2025 / Published online: 26 May 2025
© The Author(s), under exclusive licence to China Science Publishing & Media Ltd. (Science Press), Shanghai Institute of Applied Physics, the Chinese Academy of Sciences, Chinese Nuclear Society 2025

Abstract

This study explores the phenomenon of shape coexistence in nuclei around ^{172}Hg, with a focus on the isotopes ^{170}Pt, ^{172}Hg, and ^{174}Pb, as well as the ^{170}Pt to ^{180}Pt isotopic chain. Utilizing a macro-microscopic approach that incorporates the Lublin–Strasbourg Drop model combined with a Yukawa-Folded potential and pairing corrections, we analyze the potential energy surfaces (PESs) to understand the impact of pairing interaction. For ^{170}Pt, the PES exhibited a prolate ground state, with additional triaxial and oblate-shaped isomers. In ^{172}Hg, the ground-state deformation transitions from triaxial to oblate with increasing pairing interaction, demonstrating its nearly γ-unstable nature. Three shape isomers (prolate, triaxial, and oblate) were observed, with increased pairing strength leading to the disappearance of the triaxial isomer. ^{174}Pb exhibited a prolate ground state that became increasingly spherical with stronger pairing. While shape isomers were present at lower pairing strengths, robust shape coexistence was not observed. For realistic pairing interaction, the ground-state shapes transitioned from prolate in ^{170}Pt to a coexistence of γ-unstable and oblate shapes in ^{172}Hg, ultimately approaching spherical symmetry in ^{174}Pb. A comparison between Exact and Bardeen–Cooper–Schrieffer (BCS) pairing demonstrated that BCS pairing tends to smooth out shape coexistence and reduce the depth of the shape isomer, leading to less pronounced deformation features. The PESs for even–even $^{170-180}$Pt isotopes revealed significant shape evolution. ^{170}Pt showed a prolate ground state, whereas ^{172}Pt exhibited both triaxial and prolate shape coexistence. In ^{174}Pt, the ground state was triaxial, coexisted with a prolate minimum. For ^{176}Pt, a γ-unstable ground state coexists with a prolate minimum. By ^{178}Pt and ^{180}Pt, a dominant prolate minimum emerged. These results highlight the role of shape coexistence and γ-instability in the evolution of nuclear structure, especially in the mid-shell region. These findings highlight the importance of pairing interactions in nuclear deformation and shape coexistence, providing insights into the structural evolution of mid-shell nuclei.

Keywords Macro-micro-model · Shape coexistence · Shape isomers · Exact and BCS pairing solutions

1 Introduction

Shape coexistence in atomic nuclei has garnered significant attention in the field of nuclear physics and has become a prominent topic in contemporary research. This phenomenon refers to the presence of multiple distinct shapes within a single nucleus, where states with similar energies exhibit different deformations [1]. Understanding nuclear shapes is crucial for revealing the internal structure and properties of nuclei, providing tools for predicting and explaining nuclear behaviors, and advancing nuclear physics [2–6].

The study of nuclear shapes has a long history, with several foundational studies laying the groundwork for our current understanding. Early theoretical developments included Rainwater's 1950 paper [7], which first proposed the idea of nuclear deformation, and Bohr and Mottelson's collective model [8, 9], which provided a framework for describing

This work was supported by the National Natural Science Foundation of China (Nos.12275115 and 12175097) and the National Science Centre of Poland (No. 2023/49/B/ST2/01294).

✉ Xin Guan
guanxin@lnnu.edu.cn

[1] School of Physics and Electronic Technology, Liaoning Normal University, Dalian 116029, China

[2] Institute of Physics, Maria Curie Skłodowska University, 20-031 Lublin, Poland

[3] National Centre for Nuclear Research, 02-093 Warsaw, Poland

rotational spectra in deformed nuclei. Arima and Horie's 1954 study [10] explored the role of configuration mixing in nuclear structure, while Nilsson's work [11] introduced a shell-model approach incorporating deformation effects. Around the same time, Morinaga's 1956 paper [12] specifically addressed the structure of ^{16}O and explained the properties of its first excited state and ground state. He introduced the concept of multi-nucleon cross-shell excitation to describe the deformation characteristics, offering a new perspective on how nuclear shapes evolve. Further developments include Elliott's work in 1958 [13], which further developed the concept of SU(3) symmetry in nuclear deformation and highlighted the interplay between single particle and collective motion. Over the past five decades, shape coexistence has evolved from a rare phenomenon to a common feature observed in many nuclei, highlighting its significance in nuclear structure research [14]. Recent experimental studies have revealed significant evidence of shape coexistence phenomena in neutron-deficient isotopes of lead and mercury. For instance, one study [15] specifically focuses on the ^{188}Hg isotope, where theoretical predictions suggest the presence of shape coexistence.

These findings have led to increased theoretical investigations into nuclear shape coexistence, utilizing advanced experimental techniques such as tagging techniques at the University of Jyväskylä, Coulomb-excitation experiments at CERN, and relativistic energy-fragmentation experiments at GSI [16]. These experiments underscore the importance of understanding the mechanisms governing the evolution of nuclear shape. Building upon these experimental insights, theoretical investigations have played a pivotal role in elucidating the complexities of shape coexistence [17–19]. Previous studies have employed various theoretical frameworks, including macro-microscopic approaches and self-consistent models, to perform comprehensive calculations of nuclear ground-state masses and deformations across a wide range of nuclei [14]. Ref. [20] highlighted the presence of two distinct coexisting configurations, in platinum isotopes $^{176-186}$Pt, oblate and prolate, revealing the intricate shape evolution in this mass region. Therefore, shape coexistence in even–even $^{172-200}$Hg isotopes was comprehensively studied using the interacting boson model with configuration mixing [21]. Recently, using the Lublin–Strasbourg Drop (LSD) with Yukawa-Folded single-particle potential and the BCS pairing correction in a macro-microscopic model, Pomorski et al. provided the deformation PESs of nuclei near $Z = 82$. Their study investigated the shape coexistence phenomenon in even–even isotopes of Pt, Hg, and Pb [22]. These studies revealed that nuclei in the vicinity of Hg exhibit a rich variety of shape coexistence phenomena, characterized by the interplay of spherical, oblate, and prolate configurations. Although significant progress has been made in understanding these features of heavier isotopes, lighter isotopes of Hg, Pt, and Pb have been relatively underexplored owing to the scarcity of experimental data [23]. To address this gap, further theoretical investigations are crucial, as they can illuminate the evolution of shape coexistence in these lighter isotopes. Such efforts would not only enhance our theoretical understanding but also provide valuable guidance for future experimental measurements, enabling better interpretation of the limited or ambiguous data that are currently available.

Despite its success, the BCS method [24], as well as the more refined Hartree–Fock–Bogolyubov (HFB) approach, faces limitations due to the small number of valence nucleons under the pairing correlation's influence [25–31]. These methods often fail to conserve particle numbers, leading to inaccuracies in describing higher-lying excited states [32]. Alternatives such as the shell model provide successful descriptions but are limited by the combinatorial growth of model space sizes, necessitating truncation schemes for heavy nuclei and often being constrained by computational resources [33]. Recent advancements in shell-model truncation techniques, such as the Monte Carlo shell model [34] and angular momentum-projected number-conserved BCS approach [35], have made significant progress in describing deformed nuclei in heavy mass regions, offering improved computational feasibility while maintaining accuracy.

The Exact solution to the standard pairing problem, first obtained by Richardson and now referred to as the Richardson–Gaudin method, offers a promising approach for the microscopic treatment of clustering in heavy nuclei [36–43]. This method is particularly suitable for handling the large model spaces and the pairing and shell effects necessary for accurately describing heavy nuclei [44–48]. In our previous work, the deformed mean-field plus pairing model within the Richardson–Gaudin method was used to explore the quantum phase transition around neutron number $N \approx 90$ in the $A \approx 150$ mass region [49]. The analysis demonstrated the critical behavior of the shape phase transition driven by competition between deformation and pairing interactions. More recently, a new iterative algorithm was developed to find the Exact solution to the standard pairing problem within the Richardson–Gaudin method [50], which has shown excellent agreement with experimental data when applied to actinide fission nuclei isotopes [51–53].

The aim of the current study is to extend this line of inquiry by presenting a systematic study of PESs for even–even Pt, Hg, and Pb isotopes near $Z = 82$. Our investigation leverages recent advancements in shape parametrization and adopted a macro-microscopic approach, integrating the LSD model with a Yukawa-Folded single-particle potential. The analysis focuses on the impact of pairing interactions on the shape coexistence of ^{170}Pt, ^{172}Hg, ^{174}Pb nuclei, as well as $^{170-180}$Pt even–even isotopes.

2 Theoretical framework and numerical details

2.1 Deformed mean-field plus standard pairing model

The Hamiltonian of the deformed mean-field plus standard pairing model for either the proton or the neutron sector is given by

$$\hat{H} = \sum_{i=1}^{n} \varepsilon_i \hat{n}_i - G \sum_{ii'} S_i^+ S_{i'}^-, \tag{1}$$

where the sums run over all given i-double degeneracy levels of total number n, $G > 0$ is the overall pairing interaction strength, $\{\varepsilon_i\}$ are the single-particle energies obtained from mean-field, such as Hartree–Fock, Woods–Saxon potential, Yukawa-Folded single-particle potential, or Nilsson model. $n_i = a_{i\uparrow}^\dagger a_{i\uparrow} + a_{i\downarrow}^\dagger a_{i\downarrow}$ is the fermion number operator for the i-th double degeneracy level, and $S_i^+ = a_{i\uparrow}^\dagger a_{i\downarrow}^\dagger$ [$S_i^- = (S_i^+)^\dagger = a_{i\downarrow} a_{i\uparrow}$] is the pair creation (annihilation) operator, The up and down arrows in these expressions refer to time-reversed states.

According to the Richardson–Gaudin method [36–43], the Exact k-pair eigenstates of (1) with $\nu_{i'} = 0$ for even systems or $\nu_{i'} = 1$ for odd systems, in which i' is the label of the double degeneracy level that is occupied by an unpaired single particle can be written as

$$|k;\xi;\nu_{i'}\rangle = S^+(x_1^{(\xi)}) S^+(x_2^{(\xi)}) \cdots S^+(x_k^{(\xi)}) |\nu_{i'}\rangle, \tag{2}$$

where $|\nu_{i'}\rangle$ is the pairing vacuum state with the seniority $\nu_{i'}$ that satisfies $S_i^-|\nu_{i'}\rangle = 0$, and $\hat{n}_i|\nu_{i'}\rangle = \delta_{ii'}\nu_i|\nu_{i'}\rangle$ for all i. Here, ξ is an additional quantum number for distinguishing different eigenvectors with the same quantum number k and

$$S^+(x_\mu^{(\xi)}) = \sum_{i=1}^{n} \frac{1}{x_\mu^{(\xi)} - 2\varepsilon_i} S_i^+, \tag{3}$$

in which the spectral parameters $x_\mu^{(\xi)}$ ($\mu = 1, 2, \ldots, k$) satisfy the following set of Bethe ansatz equations (BAEs):

$$1 + G \sum_i \frac{\Omega_i}{x_\mu^{(\xi)} - 2\varepsilon_i} - 2G \sum_{\mu'=1(\neq\mu)}^{k} \frac{1}{x_\mu^{(\xi)} - x_{\mu'}^{(\xi)}} = 0, \tag{4}$$

where the first sum runs over all i levels and $\Omega_i = 1 - \delta_{ii'}\nu_{i'}$. For each solution, the corresponding eigenenergy is given by

$$E_k^{(\xi)} = \sum_{\mu=1}^{k} x_\mu^{(\xi)} + \nu_{i'}\varepsilon_{i'}. \tag{5}$$

In general, according to the polynomial approach in Refs. [45–48], one can find solutions of Eq. (4) by solving the second-order Fuchsian equation [44] as

$$A(x)P''(x) + B(x)P'(x) - V(x)P(x) = 0, \tag{6}$$

where $A(x) = \prod_{i=1}^{n}(x_\mu^{(\xi)} - 2\varepsilon_i)$ is an n-degree polynomial,

$$B(x)/A(x) = -\sum_{i=1}^{n} \frac{\Omega_i}{x_\mu^{(\xi)} - 2\varepsilon_i} - \frac{1}{G}, \tag{7}$$

$V(x)$ are called Van Vleck polynomials [44] of degree $n-1$, which are determined according to Eq. (6). They are defined as

$$V(x) = \sum_{i=0}^{n-1} b_i x^i. \tag{8}$$

The polynomials $P(x)$ with zeros corresponding to the solutions of Eq. (4) is defined as

$$P(x) = \prod_{i=1}^{k}(x - x_i^{(\xi)}) = \sum_{i=0}^{k} a_i x^i, \tag{9}$$

where k is the number of pairs. b_i and a_i are the expansion coefficients to be determined instead of the Richardson variables x_i. Furthermore, if we set $a_k = 1$ in $P(x)$, the coefficient a_{k-1} then equals the negative sum of the $P(x)$ zeros, $a_{k-1} = -\sum_{i=1}^{k} x_i^{(\xi)} = -E_k^{(\xi)}$.

If the value of x approaches twice the single-particle energy of a given level δ, i.e., $x = 2\varepsilon_\delta$, one can rewrite Eq. (6) in doubly degenerate systems with $\Omega_i = 1$ as [45, 46, 48]

$$\left(\frac{P'(2\varepsilon_\delta)}{P(2\varepsilon_\delta)}\right)^2 - \frac{1}{G}\left(\frac{P'(2\varepsilon_\delta)}{P(2\varepsilon_\delta)}\right) = \sum_{i\neq\delta} \frac{\left[\left(\frac{P'(2\varepsilon_\delta)}{P(2\varepsilon_\delta)}\right) - \left(\frac{P'(2\varepsilon_i)}{P(2\varepsilon_i)}\right)\right]}{2\varepsilon_\delta - 2\varepsilon_i}. \tag{10}$$

In Ref. [50], a new iterative algorithm is established for the exact solution of the standard pairing problem within the Richardson–Gaudin method using the polynomial approach in Eq. (10). It provides efficient and robust solutions for both spherical and deformed systems at a large scale. The key to its success is determining the initial guesses for the large-set nonlinear equations involved in a controllable and physically motivated manner. Moreover, one reduces the large-dimensional problem to a one-dimensional Monte Carlo sampling procedure, which improves the algorithm's efficiency and avoids the nonsolutions and numerical instabilities that persist in most existing approaches. Based on the new iterative algorithm, we applied the model to study the actinide nuclei isotopes, where an excellent agreement with experimental data was obtained [50–53].

2.2 The Fourier shape parametrization

Recent studies demonstrated that the developed Fourier parametrization of deformed nuclear shapes was highly effective in capturing the essential features of nuclear shapes, particularly up to the scission configuration [22, 54]. Current research indicated that combining this innovative Fourier shape parametrization with the LSD + Yukawa-Folded macro-microscopic potential energy framework was exceptionally efficient [52, 53, 55, 56]. This work primarily adopted the macro-microscopic framework outlined in Refs. [52, 53], where the single-particle energies $\{\epsilon_i\}$ in the model Hamiltonian (1) were derived from the Yukawa-Folded potential.

The nuclear surface is expanded in terms of a Fourier series of dimensionless coordinates as follows:

$$\frac{\rho_s^2(z)}{R_0^2} = \sum_{n=1}^{\infty}\Big[a_{2n}\cos\Big(\frac{(2n-1)\pi}{2}\frac{z-z_{sh}}{z_0}\Big) + a_{2n+1}\sin\Big(\frac{2n\pi}{2}\frac{z-z_{sh}}{z_0}\Big)\Big], \tag{11}$$

where $\rho_s(z)$ is the distance from a surface point to the symmetry z-axis, and $R_0 = 1.2A^{1/3}$ fm is the radius of a corresponding spherical shape with the same volume. The shape's extension along the symmetry axis is $2z_0$, with the left and right ends located at $z_{min} = z_{sh} - z_0$ and $z_{max} = z_{sh} + z_0$, respectively. The parameter z_0 represents half the shape's extension along the symmetry axis and is determined by volume conservation, while z_{sh} is set such that the center of mass of the nuclear shape is at the origin of the coordinate system. Based on the convergence properties discussed in Ref. [22], the first five terms $a_2, \ldots, a_6$ are retained as a starting point, and the parameters a_n are transformed into deformation parameters q_n as follows:

$$\begin{aligned} q_2 &= a_2^{(0)}/a_2 - a_2/a_2^{(0)},\\ q_3 &= a_3,\\ q_4 &= a_4 + \sqrt{(q_2/9)^2 + (a_4^{(0)})^2},\\ q_5 &= a_5 - (q_2-2)a_3/10,\\ q_6 &= a_6 - \sqrt{(q_2/100)^2 + (a_6^{(0)})^2}, \end{aligned} \tag{12}$$

where $a_n^{(0)}$ are the Fourier coefficients for the spherical shape. Higher-order coordinates q_5 and q_6 are generally set to zero within the accuracy of the current approach. The set of q_i parameters has explicit physical significance in describing the shape of the fissioning nucleus: q_2 denotes the elongation, q_4 represents the neck parameter, and q_3 indicates the left-right asymmetry.

Additionally, the non-axial deformation of nuclear shapes is described as follows, assuming that the surface cross section at a given z-coordinate is elliptical with semi-axes $a(z)$ and $b(z)$:

$$\rho_s^2(z,\varphi) = \rho_s^2(z)\frac{1-\eta^2}{1+\eta^2+2\eta\cos(2\varphi)}, \tag{13}$$

where $\eta = \frac{b-a}{b+a}$ characterizes the non-axial deformation. Volume conservation requires that $\rho_s^2(z) = a(z) + b(z)$, with the condition $ab = \rho_s^2(z)$ ensuring volume conservation for non-axial deformations. The semi-axes are then given by:

$$a(z) = \rho_s(z)\sqrt{\frac{1-\eta}{1+\eta}}, \quad b(z) = \rho_s(z)\sqrt{\frac{1+\eta}{1-\eta}}. \tag{14}$$

This description of non-axial shapes using the parameters q_2 and η is more general than the commonly used Bohr parametrization (β, γ). For spheroidal shapes, both descriptions are equivalent. However, as shown in Fig. 1, where the two parametrizations are compared, the periodicity of nuclear shapes by a 60° rotation angle is similar in both (q_2, η) and (β, γ) planes. It is important to note that this regularity is disrupted when higher multipolarity deformations q_n $(n > 2)$ are considered, making the $(\eta, q_2, q_3, q_4, q_6)$ shape parametrization substantially more general than the three-dimensional $(\epsilon_2, \epsilon_4(\gamma), \gamma)$ parametrization used in Ref. [59, 60]. The two parametrizations coincide only in the special case of spheroidal shapes.

It is essential to stress that different points in the (β, γ), and (q_2, η) planes can correspond to identical shapes when higher q_n $(n > 2)$ degrees of freedom are neglected, differing only in the interchange of coordinate system axes. For example, the point $(\beta = 0.4, \gamma = 0)$ corresponds to $(q_2 = 0.42, \eta = 0)$ in the new parametrization, representing

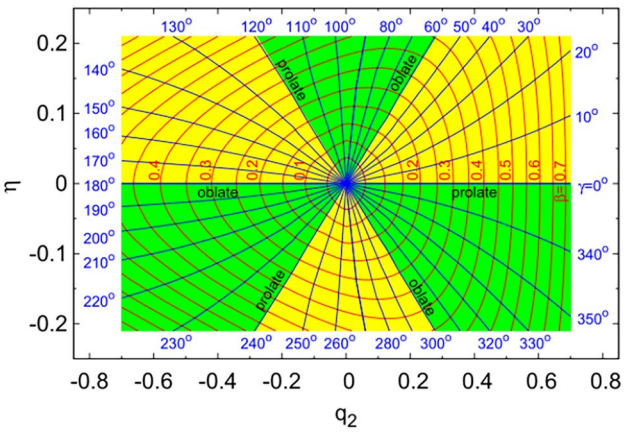

Fig. 1 (Color online) Relationship between the elongation parameter q_2 and the nonaxiality parameter η [22, 54], and the traditional Bohr deformation parameters β and γ is taken from [57, 58]

the same shape as ($\beta = 0.4, \gamma = 120°$), which corresponds to ($q_2 = -0.21, \eta = 0.16$) in the new parametrization.

When analyzing potential energy landscapes that include triaxial degrees of freedom, it is crucial to avoid treating as distinct configurations points in the (q_2, η) deformation plane that are merely rotational images of each other at $\gamma = 60°$.

In this study, the dynamic process of nuclear fission will be described in the three-dimensional deformation space (η, q_2, q_4) using the Fourier shape parametrization.

2.3 The potential energy

This study calculated the PESs for the isotopes ^{170}Pt, ^{172}Hg, and ^{174}Pb in a three-dimensional deformation space (η, q_2, q_4) and analyzed the impact of pairing interactions on the shape coexistence of these isotopes. The results were obtained over the following grid points in the deformation parameter space:

$$\begin{aligned} \eta &\in [0.00, 0.20] \qquad \Delta\eta = 0.02 \\ q_2 &\in [-0.60, 0.85] \qquad \Delta q_2 = 0.05 \\ q_4 &\in [-0.30, 0.30] \qquad \Delta q_4 = 0.03. \end{aligned} \tag{15}$$

As indicated in the literature [22], the q_3 degree of freedom has no significant impact on the description of shape coexistence for the isotopes discussed in this paper. Therefore, in this study, q_3 was set to 0, and for each point on the PES, q_4 was minimized to find the energy extremum. The potential energy of the system was calculated within the macro-microscopic approach in this work. The total energy $E_{\text{total}}(N, Z, q_n)$ of a nucleus with a given deformation is calculated as

$$E_{\text{total}}(N, Z, q_n) = E_{\text{LD}}(N, Z, q_n) + E_{\text{B}}(N, Z, q_n), \tag{16}$$

where $E_{\text{LD}}(N, Z, q_n)$ was the macroscopic term obtained by the LSD model with proton number Z and neutron number N [61]. In the current calculation for the potential energy surface, we just considered the energy $E_{\text{B}}(N, Z, q_n)$ related to the shape parameter $\{q_2, q_4\}$.

$$E_{\text{B}}(N, Z, q_n) = E_{\text{shell}}(N, Z, q_n) + E_{\text{pair}}(N, Z, q_n). \tag{17}$$

The microscopic term consisted of the shell correction energy $E^{\nu(\pi)}_{\text{shell}}(N, Z, \{\varepsilon_i\}, q_2, q_4)$ proposed by Strutinsky [62, 63], and the pairing interaction energy $E^{\nu(\pi)}_{\text{pair}}(N, Z, \{\varepsilon_i\}, q_2, q_4)$ calculated from Eq. (1). Here, ν (π) was the label of the neutron (proton) sector. In the current study, we considered 18 deformed harmonic-oscillator shells in Yukawa-Folded single-particle potential to obtain single-particle levels for the microscopic calculations. For the pairing interaction energy, we performed 29 single-particle levels around the neutron Fermi level and 22 single-particle levels around the proton Fermi level.

To validate our results and further explored the efficacy of the exactly solvable pairing model, we also calculated the PESs for the isotopes considered under the BCS approximation. The pairing interaction was determined as the difference between the BCS energy [24] and the single-particle energy sum and the average pairing energy [64].

$$E_{\text{pair}} = E_{\text{BCS}} - \sum_{i=1}^{k} \varepsilon_i - \widetilde{E}_{\text{pair}}. \tag{18}$$

In the BCS approximation the ground-state energy of a system with an even number of particles and a monopole pairing force was given by

$$E_{\text{BCS}} = \sum_{i=1}^{k} 2\varepsilon_i v_k^2 - G\left(\sum_{i=1}^{k} u_i v_i\right)^2 - G\sum_{i=1}^{k} v_i^4, \tag{19}$$

where the sums run over the pairs of single-particle states contained in the pairing window defined below. The coefficients v_i and $u_i = \sqrt{1 - v_i^2}$ were the BCS occupation amplitudes.

The average projected pairing energy, for a pairing window of width 2Ω, which is symmetric in energy with respect to the Fermi energy, is equal to

$$\begin{aligned} \widetilde{E}_{\text{pair}} = &-\frac{1}{2}\tilde{g}\tilde{\Delta}^2 + \frac{1}{2}\tilde{g}G\tilde{\Delta}\arctan\left(\frac{\Omega}{\tilde{\Delta}}\right) - \log\left(\frac{\Omega}{\tilde{\Delta}}\right)\tilde{\Delta} \\ &+ \frac{3}{4}G\frac{\Omega/\tilde{\Delta}}{1 + \left(\Omega/\tilde{\Delta}\right)^2} \Big/ \arctan\left(\frac{\Omega}{\tilde{\Delta}}\right) - \frac{1}{4}G. \end{aligned} \tag{20}$$

Here $\tilde{g}$ was the average single-particle level density and $\tilde{\Delta}$ the average paring gap corresponding to a pairing strength G

$$\tilde{\Delta} = 2\Omega\exp\left(-\frac{1}{G\tilde{g}}\right). \tag{21}$$

2.4 Influence of pairing interactions on the shape coexistence of ^{170}Pt, ^{172}Hg and ^{174}Pb isotopes

Figure 2 shows the PESs of ^{170}Pt projected onto the (q_2, η) plane for different pairing interaction strengths G^{ν} (MeV), while the proton pairing interaction strength is fixed at $G^{\pi} = 0.100$ MeV. G^{ν} and G^{π} represent the neutron and proton pairing interaction strengths (MeV), respectively. The energy is minimized in the q_4 direction, and q_3 is set to 0 and normalized to zero energy at the ground-state value. The choice of G^{ν} varying from 0.03 to 0.145 MeV, and $G^{\pi} = 0.100$ MeV, were based on the fact that our calculations in the next section, when employing $G^{\nu} = 0.145$ MeV, and $G^{\pi} = 0.100$ MeV, closely matched the experimental odd–even mass differences for the ^{171}Pt to ^{180}Pt isotopes. Therefore, this range was selected to study the effects of

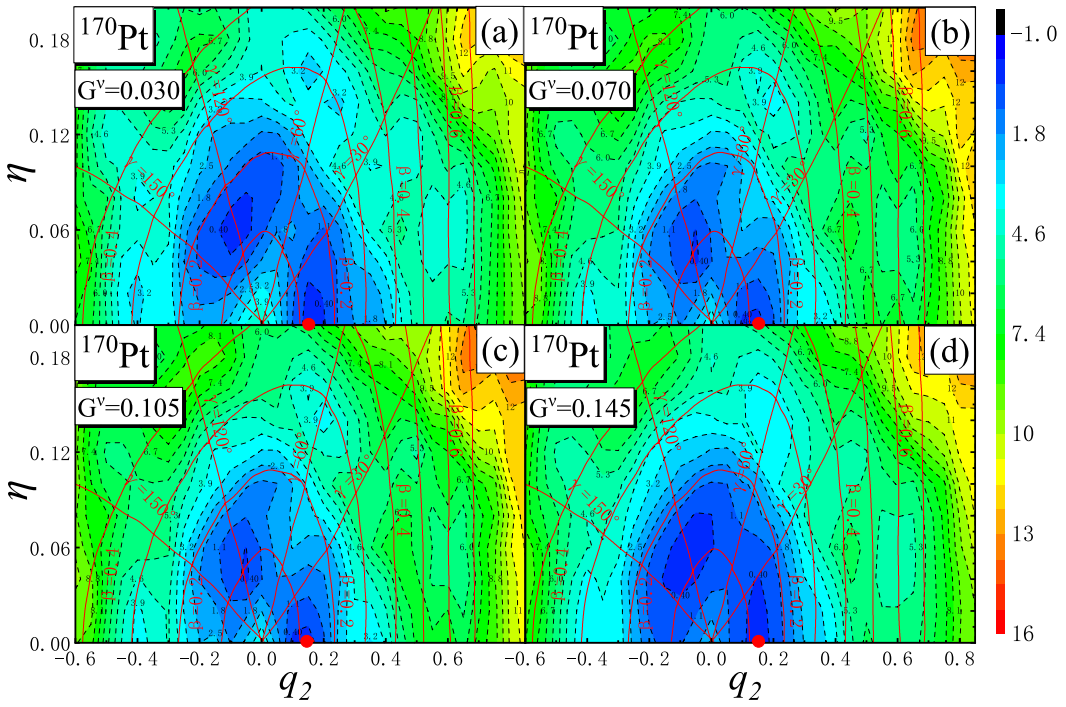

Fig. 2 (Color online) Potential energy surface of ^{170}Pt projected onto the (q_2, η) plane under different pairing interaction strengths G^{ν} (MeV), while the proton pairing interaction strength is fixed at $G^{\pi} = 0.100$ MeV. The energy is minimized in the q_4 direction, and q_3 is set to 0 and normalized to zero energy at the ground-state value. The ground-state deformation is represented by a red dot

pairing strength variations on the shape coexistence. The red lines represent the corresponding (β, γ) coordinates, with γ coordinates distributed within $0 \leq \gamma \leq 180°$. The β coordinate values are taken as $0.1, 0.2, 0.3 \ldots$, etc.

In Fig. 2a–d, the PESs of ^{170}Pt are shown for different values of the neutron pairing interaction strength G^{ν}, while the proton pairing interaction strength is fixed at $G^{\pi} = 0.100$ MeV. The values of G^{ν} are: 0.030, 0.070, 0.105, and 0.145 MeV. It can be seen that the ground state of the ^{170}Pt isotope is located at $(q_2 \approx 0.150, \eta = 0)$, indicating a prolate shape for different pairing strengths. The other minimum at $(q_2 \approx -0.150, \eta = 0.04, \gamma = 120°)$ illustrated in Fig. 2 is simply a reflection of the ground-state minimum.

It is noteworthy to highlight the existence of two distinct shape isomers in ^{170}Pt with different pairing strengths. The first is an oblate shape isomer located at $(q_2 = -0.400, \eta = 0)$, with an energy approximately 3.900 MeV above the ground state. The second is a triaxial shape isomer at $(q_2 \approx 0.600, \eta \approx 0.060\ (\gamma \approx 10°))$, positioned around 4.0 MeV above the ground state. These isomers represent the local minima on the potential energy surface that are separated from the ground state by energy barriers, highlighting the complex deformation characteristics of the nucleus. With an increase in pairing strength, both shape isomers become shallower. When the pairing strength G^{ν} reaches 0.145 MeV, the oblate isomer disappears (see Fig. 2d).

As shown in Fig. 3a–d, the PESs for different pairing interaction strengths demonstrates the evolution of the triaxial minimum at $(q_2 = 0.150, \eta = 0.020)$ to the oblate minimum at $(q_2 = 0.100, \eta = 0.040)$ as the pairing interaction strength increases. The nucleus of ^{172}Hg is nearly γ-unstable, with the energy difference between different points in the ground-state valley not exceeding approximately 0.4 MeV. Additionally, three shape isomers are visible in the (a)-(d) maps: a prolate isomer at $(q_2 \approx 0.600, \eta = 0)$, $E \approx 5.0$ MeV; a triaxial isomer at $(q_2 \approx 0.400, \eta = 0.100)$, $E \approx 4.0$ MeV; and oblate one at $(q_2 \approx -0.45, \eta = 0)$, $E \approx 4.0$ MeV. These local minima are separated by energy barriers of approximately 1 MeV in height. As the pairing strength increases, all shape isomers gradually become shallower. By $G^{\nu} = 0.145$ MeV and $G^{\pi} = 0.100$ MeV (Fig. 3d), the triaxial isomer at $(q_2 \approx 0.400, \eta = 0.100)$ disappeared.

The PESs of ^{174}Pb, as presented in Fig. 4a–d, reveal that a prolate ground state $(q_2 \approx 0.150, \eta = 0)$ (in Fig. 4a) tends to become spherical (in Fig. 4d) as the pairing interaction strength increases. The shape isomers observed here are particularly interesting: a prolate shape at $(q_2 = 0.600, \eta = 0)$, $E \approx 5.0$ MeV and a slightly triaxial oblate shape at $(q_2 = 0.450, \eta = 0.020)$, $E \approx 3.9$ MeV in Fig. 4a, b, respectively. As the pairing strength increased,

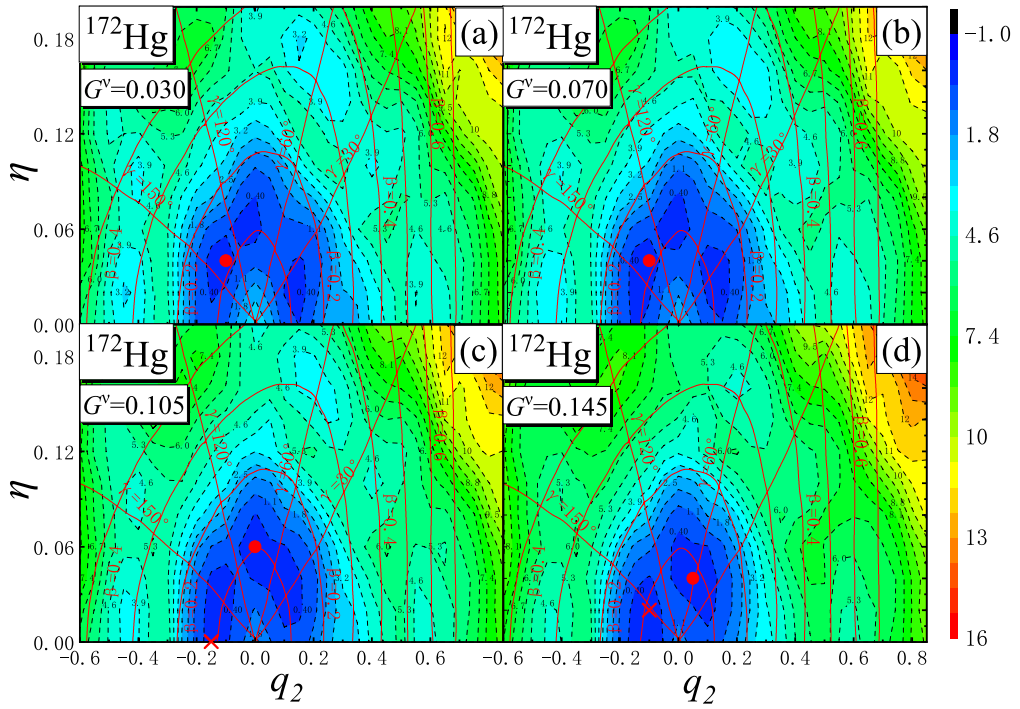

Fig. 3 (Color online) Same as Fig. 2, but for ^{172}Hg

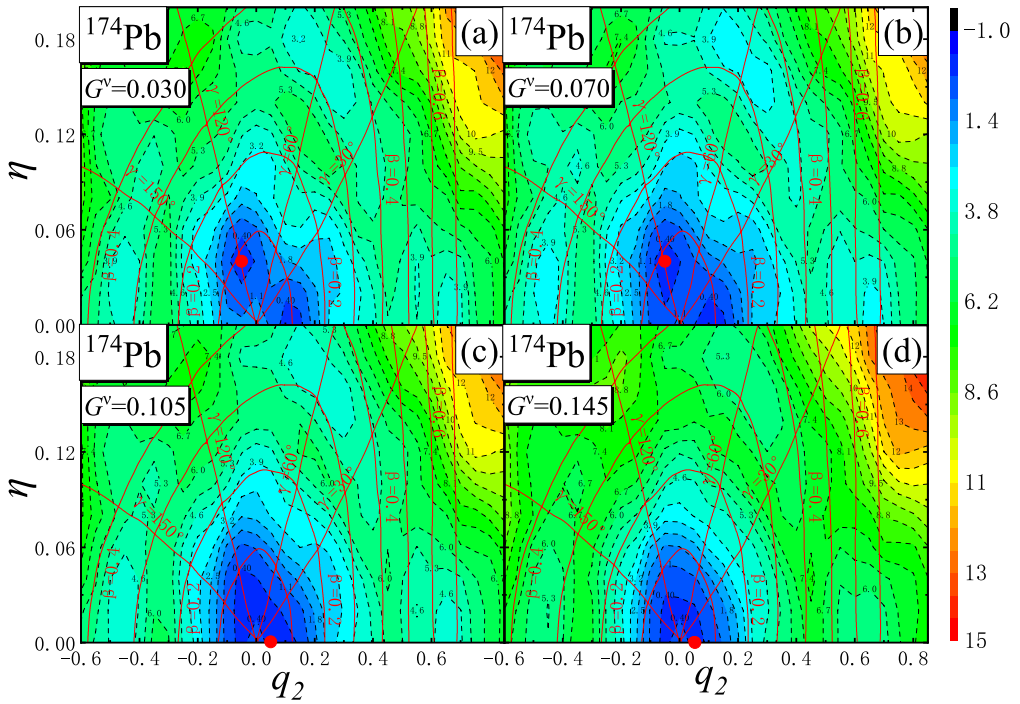

Fig. 4 (Color online) Same as Figs. 2 and 3, but for ^{174}Pb

both shape isomers gradually became shallower. When $G^{\nu} = 0.145$ MeV, and $G^{\pi} = 0.100$ MeV (Fig. 4d), they almost disappeared. Overall, regardless of pairing strength, there was no indication of robust shape coexistence in this nucleus.

Figure 5 illustrates the PESs projections of ^{170}Pt, ^{172}Hg, and ^{174}Pb under realistic pairing interaction strengths, with $G^{\nu} = 0.145$ MeV, and $G^{\pi} = 0.100$ MeV under both Exact and BCS pairing schemes.

As shown in Fig. 5, the ground state of ^{170}Pt is prolate, located at $(q_2 = 0.15, \eta = 0)$ under both the Exact and BCS pairing schemes. However, BCS pairing exhibited a shallower depth for the prolate minimum compared with Exact pairing, indicating a less pronounced prolate ground state. Furthermore, a triaxial isomer appeared at $(q_2 \approx 0.600, \eta \approx 0.060\ (\gamma \approx 10°))$ under Exact pairing, whereas it was less distinguishable in the BCS case.

The ground state of ^{172}Hg (Fig. 5) is found at $(q_2 = 0.10, \eta \approx 0.04)$ as an oblate minimum, with another minimum at $(q_2 \approx -0.100, \eta \approx 0.02)$, which exhibits γ -unstable deformation. The PES of ^{172}Hg provides an excellent example of an almost γ-unstable nucleus. Under Exact pairing, this γ-unstable minimum is more symmetric, with clear reflections around $\gamma = 150°, \gamma = 30°$, and $\gamma = 90°$. Under BCS pairing, the γ-unstable features are less prominent, and the oblate minimum becomes more dominant. Additionally, two shape isomers are visible under Exact pairing model: a prolate isomer at $(q_2 \approx 0.600, \eta = 0)$, $E \approx 4.6$ MeV, and an oblate one at $(q_2 \approx -0.45, \eta = 0)$, $E \approx 4.6$ MeV. However, these changes were not distinguishable in the BCS case.

As shown in Fig. 5c, the ground-state shape of ^{174}Pb tended to be spherical. The PES under Exact pairing revealed a nearly spherical configuration with minor prolate and oblate shape isomers. In contrast, BCS pairing resulted in a more pronounced spherical minimum and diminishes the depth of shape isomers.

In summary, as the number of protons increases, the ground-state transitions from prolate for ^{170}Pt to the coexistence of γ-unstable and oblate for ^{172}Hg, eventually approached a nearly spherical configuration for ^{174}Pb. The comparison between Exact and BCS pairing demonstrates that BCS pairing tends to smooth out shape coexistence and reduce the depth of shape isomer, leading to less pronounced deformation features. The differences in results between Exact and BCS pairing may be attributed to the mean-field approximation in the BCS approach, which likely simplifies the treatment of pairing interactions. This approximation is thought to smooth out shape coexistence phenomena by suppressing pairing fluctuations, energy gaps, and shell effects, potentially leading to less pronounced deformation features.

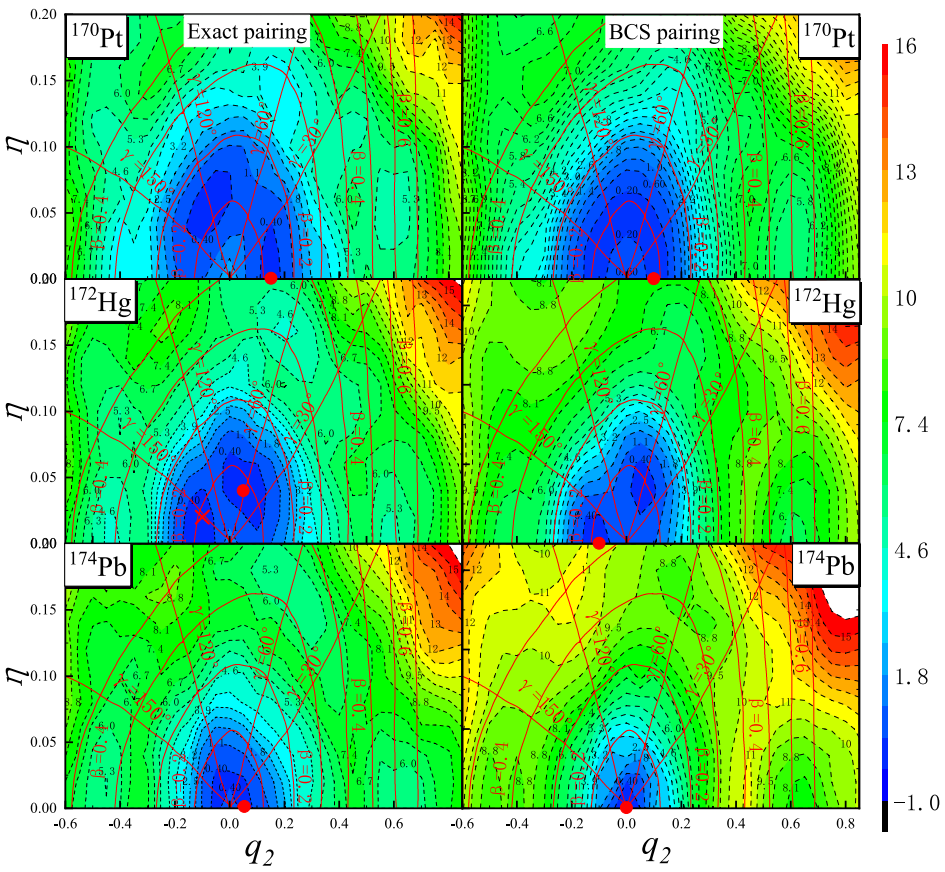

Fig. 5 (Color online) Potential energy surfaces of ^{170}Pt, ^{172}Hg and ^{174}Pb projected on the (q_2, η) plane under both Exact and BCS pairing schemes, with the energy minimized in the q_4 direction, q_3 set to 0 and normalized to zero energy at the ground-state value. The realistic pairing interaction strengths $G^{\nu} = 0.145$ MeV, and $G^{\pi} = 0.100$ MeV are adopted. The ground-state deformation is represented by a red dot, while the coexistence minimum is indicated by a red cross

2.5 Shape coexistence analysis in the Pt isotope chain

In this paper, we investigate the PESs of the even–even $^{170-180}$Pt isotopes using the exactly solvable deformed mean-field plus pairing model. Our analysis provides a comprehensive examination of the shape coexistence phenomena across these isotopes.

The pairing interaction strength, denoted as G, serves as the sole adjustable parameter within our model. It is typically determined either through empirical formulas or by fitting to experimental odd–even mass differences [65, 66]. In this study, we determined G^{ν} by fitting the experimental odd–even mass differences for the $^{171-180}$Pt isotope chain and G^{π} by fitting the experimental odd–even mass differences for the ^{174}Pt to ^{178}Pb isotonic chain. The odd–even mass differences are computed using the following expression:

$$P(A) = E_{\text{total}}(N+1,Z) + E_{\text{total}}(N-1,Z) - 2E_{\text{total}}(N,Z).$$

This quantity is highly sensitive to variations in the pairing interaction strength G [67], due to the pairing interaction between nucleons. As shown in Fig. 6, by employing $G^{\nu} = 0.145$ MeV and $G^{\pi} = 0.100$ MeV, our calculations closely reproduced the experimental odd–even mass differences for the $^{171-180}$Pt isotopes, yielding a root mean square deviation of $\sigma = 0.465$ MeV. Additionally, as displayed in Fig. 7 for the ^{174}Pt to ^{178}Pb isotonic chain, the calculations closely matched the experimental odd–even mass differences, with a root mean square deviation of $\sigma = 1.192$ MeV.

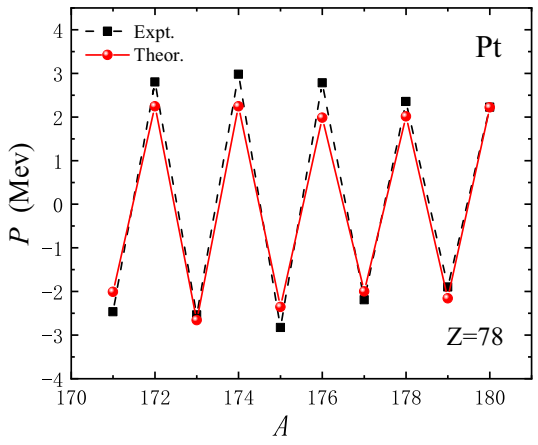

Fig. 6 Odd–even mass differences (in MeV) for Pt isotopes. "Expt." represents experimental values, and "Theor." represents theoretical values. Experimental data are from [67]

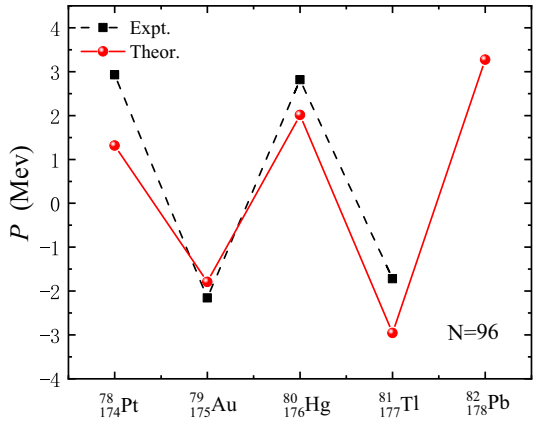

Fig. 7 Odd–even mass differences (in MeV) for the ^{174}Pt to ^{178}Pb isotonic chain. "Expt." represents experimental values, and "Theor." represents theoretical values. Experimental data are from [67]

$$\sigma = \sqrt{\sum_{\mu=1}^{\mathcal{N}} \left(P_{\mu}^{\text{Theor.}} - P_{\mu}^{\text{Expt.}}\right)^2 \Big/ \mathcal{N}}, \tag{22}$$

here, $P_{\mu}^{\text{Theor.}}$ and $P_{\mu}^{\text{Expt.}}$ represent the theoretical and experimental values of the odd–even mass differences, respectively, and $\mathcal{N}$ denotes the total number of data points.

Next, we examine the PES of the $^{170-180}$Pt even–even isotopes under the determined pairing interaction strengths $G^{\nu} = 0.145$ MeV and $G^{\pi} = 0.100$ MeV. Figure 8 shows the PES projected onto the (q_2, η) plane. For ^{170}Pt, the ground state exhibited a prolate deformation at $(q_2 = 0.15, \eta = 0)$. In contrast, for ^{172}Pt, a more deformed minimum emerged, leading to the coexistence of a triaxial shape ($\gamma \approx 30°$) and a nearly prolate-deformed minimum at ($\gamma \approx 120°$), indicative of γ-instability due to the presence of multiple low-energy configurations at different γ values. The triaxial shape is even more pronounced in ^{174}Pt, where the ground state is triaxial with deformation parameters $(q_2 = 0.020, \eta = 0.10,\ \beta \approx 0.2, \gamma \approx 90°)$ and a coexisting prolate minimum at $(q_2 = 0.15, \eta = 0)$. In ^{176}Pt a γ -unstable ground state and a prolate minimum coexisted, but by ^{178}Pt and ^{180}Pt, a well-deformed prolate minimum quickly developed, becoming the most pronounced prolate ground state at the mid-shell.

The findings of this study are broadly consistent with the results of Ref. [20], which studied the $^{172-194}$Pt isotopic chain in the framework of the interacting boson model and self-consistent HFB calculation using the Gogny-D1S interaction. Both studies identified shape coexistence in the $^{172-176}$Pt region, with γ-unstable minima and triaxial shapes in ^{174}Pt. Additionally, both studies showed the dominance of prolate deformation in ^{178}Pt, and ^{180}Pt, with the prolate minimum becoming the most pronounced ground state at the mid-shell.

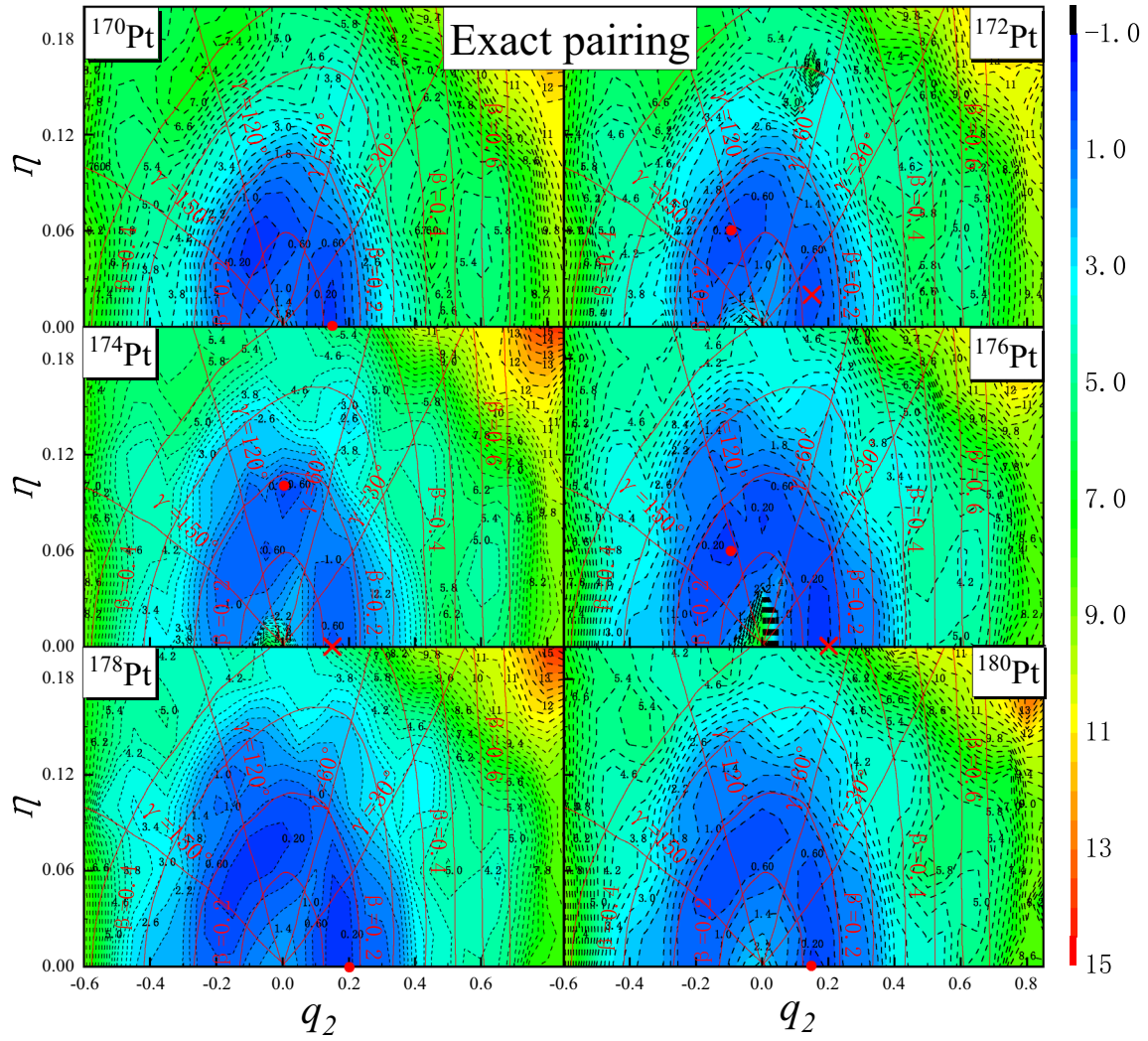

Fig. 8 (Color online) Potential energy surfaces of the $^{170-180}$Pt even–even isotopes chain, projected on the (q_2, η) plane using the Exact pairing model, where the energy is minimized in the q_4 direction with q_3 set to 0, with neutron and proton pairing interaction strengths of $G^{\nu} = 0.145$ MeV, $G^{\pi} = 0.100$ MeV. The ground-state deformation is represented by a red dot, while the coexistence minimum is indicated by a red cross

It is noteworthy that a triaxial shape isomer exists for $^{170-174}$Pt, characterized by ($q_2 \approx 0.600, \eta \approx 0.060$ ($\gamma \approx 10°$)), and positioned approximately 5.0 MeV above the ground state. However, this triaxial shape isomer vanishes for $^{176-180}$Pt.

3 Conclusion

In this study, we systematically investigated the shape coexistence phenomenon in isotopes near the magic proton number of $Z = 82$, focusing specifically on the nuclei ^{170}Pt, ^{172}Hg, and ^{174}Pb, as well as the Pt isotopic chain from ^{170}Pt to ^{180}Pt. Our analysis, using a macro-microscopic approach that combines the LSD model with a Yukawa-Folded potential and pairing corrections, revealed significant insights into the impact of pairing interactions on nuclear shape evolution.

The PES of ^{170}Pt revealed a prolate ground state with additional triaxial and oblate shape isomers. Both shape isomers become progressively shallower with increasing neutron pairing strength G^{ν}, and the oblate isomer vanishes at $G^{\nu} = 0.145$ MeV, indicating a significant dependence of shape isomers on pairing strength. The ground-state deformation of ^{172}Hg transitions from triaxial to oblate with increasing G^{ν}, reflecting its nearly γ-unstable nature. Three shape isomers (prolate, triaxial, and oblate) were observed, with energy barriers separating these configurations. As G^{ν} increased, the triaxial isomer disappeared at $G^{\nu} = 0.145$ MeV, demonstrating the impact

of pairing interactions on shape stability. ^{174}Pb exhibited a prolate ground state that became increasingly spherical with stronger pairing interactions. While shape isomers are present at weaker pairing strengths, their prominence diminishes significantly, and robust shape coexistence was not observed in this nucleus.

For realistic pairing interaction, the ground-state shapes transition from prolate in ^{170}Pt to a coexistence of γ-unstable and oblate shapes in ^{172}Hg, ultimately approaching spherical symmetry in ^{174}Pb. This progression highlights the interplay between proton number and pairing interactions in shaping nuclear deformation. The comparison between Exact and BCS pairing for realistic ^{170}Pt, ^{172}Hg, and ^{174}Pb demonstrated that BCS pairing tends to smooth out shape coexistence and reduce the depth of shape isomers, leading to less pronounced deformation features.

These findings emphasize the critical role of pairing interactions in shaping nuclear deformation landscapes and shape coexistence, offering deeper insights into the structural evolution of nuclei near the mid-shell region. This study contributes valuable theoretical perspectives to the understanding of nuclear shape phenomena and the influence of pairing interactions on nuclear dynamics.

Based on the analysis of the PESs for the even–even $^{170-180}$Pt isotopes, the results show significant shape evolution across the isotopic chain. For ^{170}Pt, the ground state exhibited prolate deformation, with deformation parameters. However, for ^{172}Pt, a more deformed minimum appears, leading to the coexistence of a triaxial shape and a nearly prolate-deformed minimum. The triaxial shape becomes even more pronounced in ^{174}Pt, where the ground state is triaxial with deformation parameters, coexisting with a prolate minimum. For ^{176}Pt, a γ-unstable ground state coexists with a prolate minimum. By ^{178}Pt, and ^{180}Pt, a well-deformed prolate minimum develops rapidly, becoming the most pronounced prolate ground state in the mid-shell.

These results highlight the complex shape evolution in the Pt isotopes, with shape coexistence and γ-instability playing significant roles in the nuclear structure evolution, particularly around the mid-shell region where prolate deformation dominates.

Author contributions All authors contributed to the study conception and design. Material preparation and data collection and analysis were performed by Jing Guo, Qi Wen Sun, and Xian Guan. The first draft of the manuscript was written by Xian Guan, and all authors commented on previous versions of the manuscript. All authors read and approved the final manuscript.

Data availability The data that support the findings of this study are openly available in Science Data Bank at https://cstr.cn/31253.11.sciencedb.j00186.00671 and https://www.doi.org/10.57760/sciencedb.j00186.00671.

Declarations

Conflict of interest The authors declare that they have no Conflict of interest.

References

1. K. Heyde, J.L. Wood, Publisher's Note: shape coexistence in atomic nuclei. Rev. Mod. Phys. **83**, 1467 (2011). https://doi.org/10.1103/RevModPhys.83.1655
2. J.Y. Jia, G. Giacalone, B. Bally et al., Imaging the initial condition of heavy-ion collisions and nuclear structure across the nuclide chart. Nucl. Sci. Tech. **35**, 220 (2024). https://doi.org/10.1007/s41365-024-01589-w
3. M.Q. Ding, D.Q. Fang, Y.G. Ma, Neutron skin and its effects in heavy-ion collisions. Nucl. Sci. Tech. **35**, 211 (2024). https://doi.org/10.1007/s41365-024-01584-1
4. B.S. Cai, C.X. Yuan, Random forest-based prediction of decay modes and half-lives of superheavy nuclei. Nucl. Sci. Tech. **34**, 204 (2023). https://doi.org/10.1007/s41365-023-01354-5
5. J.L. Huang, H. Wang, Y.G. Huang et al., Prediction of $(n, 2n)$ reaction cross-sections of long-lived fission products based on tensor model. Nucl. Sci. Tech. **35**, 184 (2024). https://doi.org/10.1007/s41365-024-01556-5
6. Y. Liu, F.R. Xu, Z.B. Cao, Shape coexistence in selenium isotopes. Nucl. Phys. Rev. **27**, 2 (2010). https://doi.org/10.11804/NuclPhysRev.27.02.146
7. J. Rainwater, Nuclear energy level argument for a spheroidal nuclear model. Phys. Rev. **79**, 432 (1950). https://doi.org/10.1103/PhysRev.79.432
8. A. Bohr, B.R. Mottelson, Collective and individual-particle aspects of nuclear structure. Dan. Mat. Fys. Medd. **27**, 16 (1953)
9. A. Bohr, B.R. Mottelson, Moments of inertia of rotating nuclei. Dan. Mat. Fys. Medd. **30**, 1 (1955)
10. A. Arima, H. Horie, Configuration mixing and magnetic moments of odd nuclei. Prog. Theor. Phys. **12**, 623 (1954). https://doi.org/10.1143/PTP.12.623
11. S.G. Nilsson, Binding states of individual nucleons in strongly deformed nuclei. Dan. Mat. Fys. Medd. **29**, 16 (1955)
12. H. Morinaga, Interpretation of some of the excited states of $4n$ self-conjugate. Phys. Rev. **101**, 254 (1956). https://doi.org/10.1103/PhysRev.101.254
13. J.P. Elliott, Collective motion in the nuclear shell model I Classification schemes for states of mixed configurations. Proc. R. Soc. A **245**, 128 (1958). https://doi.org/10.1098/rspa.1958.0072
14. P. Möller, A.J. Sierk, R. Bengtsson et al., Global calculation of nuclear shape isomers. Phys. Rev. Lett. **103**, 212501 (2009). https://doi.org/10.1103/PhysRevLett.103.212501
15. M. Siciliano, I. Zanon, A. Goasduff et al., Shape coexistence in the neutron-deficient ^{188}Hg investigated via lifetime measurements. Phys. Rev. C **102**, 014318 (2020). https://doi.org/10.1103/PhysRevC.102.014318
16. R. Julin, T. Grahn, J. Pakarinen et al., In-beam spectroscopic studies of shape coexistence and collectivity in the neutron-deficient $Z \approx 82$ nuclei. J. Phys. G. **43**, 024004 (2016). https://doi.org/10.1088/0954-3899/43/2/024004
17. M. Bender, P.H. Heenen, P.G. Reinhard, Self-consistent mean-field models for nuclear structure. Rev. Mod. Phys. **75**, 121 (2003). https://doi.org/10.1103/RevModPhys.75.121
18. T. Nikšić, D. Vretenar, P. Ring et al., Shape coexistence in the relativistic Hartree-Bogoliubov approach. Phys. Rev. C **65**, 054320 (2002). https://doi.org/10.1103/PhysRevC.65.054320

19. F.Z. Xing, J.P. Cui, Y.H. Gao et al., Structure and α decay of superheavy nucleus ^{296}Og. Nucl. Phys. Rev. **40**, 4 (2023). https://doi.org/10.11804/NuclPhysRev.40.2023059
20. J.E. García-Ramos, K. Heyde, L.M. Robledo et al., Shape evolution and shape coexistence in Pt isotopes: comparing interacting boson model configuration mixing and Gogny mean-field energy surfaces. Phys. Rev. C **98**, 034313 (2014). https://doi.org/10.1103/PhysRevC.81.024310
21. J.E. García-Ramos, K. Heyde, Nuclear shape coexistence: a study of the even-even Hg isotopes using the interacting boson model with configuration mixing. Phys. Rev. C **89**, 014306 (2014). https://doi.org/10.1103/PhysRevC.89.014306
22. K. Pomorski, B. Nerlo-Pomorska, A. Dobrowolski et al., Shape isomers in Pt, Hg and Pb isotopes with $N\leq126$. Eur. Phys. J. A **56**, 107 (2020). https://doi.org/10.1140/epja/s10050-020-00115-x
23. T. Kibedi, C.M. Baglin, ENSDEF (2010), http://www.nndc.bnl.gov/ensdf
24. J. Bardeen, L.N. Cooper, J.R. Schrieffer, Theory of superconductivity. Phys. Rev. **108**, 1175 (1957). https://doi.org/10.1103/PhysRev.108.1175
25. A. Bohr, B.R. Mottelson, D. Pines, Possible analogy between the excitation spectra of nuclei and those of the superconducting metallic state. Phys. Rev. **110**, 4 (1958). https://doi.org/10.1103/PhysRev.110.936
26. S.T. Belyaev, Effect of pairing correlations on nuclear properties. Dan. Mat. Fys. Medd. **31**, 11 (1959)
27. Y.Z. Wang, F.Z. Xing, J.P. Cui et al., Roles of tensor force and pairing correlation in two-proton radioactivity of halo nuclei. Chin. Phys. C **47**, 084101 (2023). https://doi.org/10.1088/1674-1137/acd680
28. Y.Z. Wang, F.Z. Xing, W.H. Zhang et al., Tensor force effect on two-proton radioactivity of ^{18}Mg and ^{20}Si. Phys. Rev. C **110**, 064305 (2024). https://doi.org/10.1103/PhysRevC.110.06430
29. Y.Z. Wang, L. Yang, C. Qi et al., Pairing effects on bubble nuclei. Chin. Phys. Lett. **36**, 032101 (2019). https://doi.org/10.1088/0256-307X/36/3/032101
30. Y.Z. Wang, Z.Y. Hou, Q.L. Zhang et al., Effect of a tensor force on the proton bubble structure of ^{206}Hg. Phys. Rev. C **91**, 017302 (2015). https://doi.org/10.1103/PhysRevC.91.017302
31. J. Rissanen, R.M. Clark, A.O. Macchiavelli et al., Effect of the reduced pairing interaction on α-decay half-lives of multi-quasiparticle isomeric states. Phys. Rev. C **90**, 044324 (2014). https://doi.org/10.1103/PhysRevC.90.044324
32. N. Sandulescu, G.F. Bertsch, Accuracy of BCS-based approximations for pairing in small Fermi systems nuclei. Phys. Rev. C. **78**, 064318 (2008). https://doi.org/10.1103/PhysRevC.78.064318
33. I. Talmi, Simple Models of Complex Nuclei. (Harwood Academic Publishers, Switzerland) (1993). https://doi.org/10.1201/9780203739716
34. T. Otsuka, Y. Tsunoda, T. Abe et al., Underlying structure of collective bands and self-organization in quantum systems. Phys. Rev. Lett. **123**, 222502 (2019). https://doi.org/10.1103/PhysRevLett.123.222502
35. Y.X. Yu, Y. Lu, G.J. Fu et al., Nucleon-pair truncation of the shell model for medium-heavy nuclei. Phys. Rev. C **106**, 044309 (2022). https://doi.org/10.1103/PhysRevC.106.044309
36. R.W. Richardson, A restricted class of exact eigenstates of the pairing-force Hamiltonian. Phys. Lett. **3**, 3277 (1963). https://doi.org/10.1016/0031-9163(63)90259-2
37. R.W. Richardson, Application to the exact theory of the pairing model to some even isotopes of lead. Phys. Lett. **5**, 82 (1963). https://doi.org/10.1016/S0375-9601(63)80039-0
38. R.W. Richardson, N. Sherman, Exact eigenstates of the pairing-force Hamiltonian. Nucl. Phys. **52**, 221 (1964). https://doi.org/10.1016/0029-5582(64)90687-X
39. R.W. Richardson, N. Sherman, Pairing models of Pb^{206}, Pb^{204} and Pb^{202}. Nucl. Phys. **52**, 253 (1964). https://doi.org/10.1016/0029-5582(64)90690-X
40. M. Gaudin, Diagonalization of a class of spin Hamiltonians. Phys. J. **37**, 1087 (1976)
41. F. Pan, J.P. Draayer, W.E. Ormand, A particle-number-conserving solution to the generalized pairing problem. Phys. Lett. B **422**, 1 (1998). https://doi.org/10.1016/S0370-2693(98)00034-3
42. J. Dukelsky, C. Esebbag, S. Pittel, Electrostatic mapping of nuclear pairing. Phys. Rev. Lett. **88**, 062501 (2002). https://doi.org/10.1103/PhysRevLett88.062501
43. J. Dukelsky, S. Pittel, G. Sierra, Colloquium: exactly solvable Richardson-Gaudin models for many-body quantum systems. Rev. Mod. Phys. **76**, 643 (2004). https://doi.org/10.1103/RevModPhys.76.643
44. X. Guan, K.D. Launey, M.X. Xie et al., Heine-Stieltjes correspondence and the polynomial approach to the standard pairing problem. Phys. Rev. C **86**, 024313 (2012). https://doi.org/10.1103/PhysRevC.86.024313
45. A. Faribault, O.E. Araby, C. Sträter et al., Gaudin models solver based on the correspondence between Bethe ansatz and ordinary differential equations. Phys. Rev. B **83**, 235124 (2011). https://doi.org/10.1103/PhysRevB.83.235124
46. O. El Araby, V. Gritsev, A. Faribault, Bethe ansatz and ordinary differential equation correspondence for degenerate Gaudin models. Phys. Rev. B **85**, 115130 (2012). https://doi.org/10.1103/PhysRevB.85.115130
47. X. Guan, K.D. Launey, M.X. Xie et al., Numerical algorithm for the standard pairing problem based on the Heine-Stieltjes correspondence and the polynomial approach. Comp. Phys. Commun. **185**, 2714 (2014). https://doi.org/10.1016/j.cpc.2014.05.023
48. C. Qi, T. Chen, Exact solution of the pairing problem for spherical and deformed systems. Phys. Rev. C **92**, 051304(R) (2015). https://doi.org/10.1103/PhysRevC.92.051304
49. X. Guan, H.C. Xu, F. Pan et al., Ground state phase transition in the Nilsson mean-field plus standard pairing model. Phys. Rev. C **94**, 024309 (2016). https://doi.org/10.1103/PhysRevC.94.024309
50. X. Guan, C. Qi, An iterative approach for the exact solution of the pairing Hamiltonian. Comp. Phys. Comm. **275**, 108310 (2022). https://doi.org/10.1016/j.cpc.2022.108310
51. X. Guan, Y. Xin, Y.J. Chen et al., Impact of pairing interactions on fission in the deformed mean-field plus standard pairing model. Phys. Rev. C **104**, 044329 (2021). https://doi.org/10.1103/PhysRevC.104.044329
52. X. Guan, T.C. Wang, W.Q. Jiang et al., Impact of the pairing interaction on fission of U isotopes. Phys. Rev. C **107**, 034307 (2023). https://doi.org/10.1103/PhysRevC.107.034307
53. X. Guan, J.H. Zheng, M.Y. Zheng, Pairing effects on the fragment mass distribution of Th, U, Pu, and Cm isotopes. Nucl. Sci. Tech. **34**, 173 (2023). https://doi.org/10.1007/s41365-023-01316-x
54. C. Schmitt, K. Pomorski, B.K. Nerlo-Pomorska et al., Performance of the Fourier shape parametrization for the fission process. Phys. Rev. C **95**, 034612 (2017). https://doi.org/10.1103/PhysRevC.95.034612
55. K. Pomorski, J.M. Blanco, P.V. Kostryukov et al., Fission fragment mass yields of Th to Rf even-even nuclei. Chin. Phys. C **45**, 054109 (2021). https://doi.org/10.1088/1674-1137/abec69
56. L.L. Liu, Y.J. Chen, X.Z. Wu et al., Analysis of nuclear fission properties with the Langevin approach in Fourier shape parametrization. Phys. Rev. C **103**, 044601 (2021). https://doi.org/10.1103/PhysRevC.103.044601
57. A. Bohr, The coupling of nuclear surface oscillations to the motion of individual nucleons. Dan. Mat. Fys. Medd. **26**, 14 (1952)

58. T. Kaniowska, A. Sobiczewski, K. Pomorski et al., Microscopic inertial functions for nuclei in the barium region. Nucl. Phys. A **274**, 151 (1976). https://doi.org/10.1016/0375-9474(76)90233-5
59. S.G. Rohoziáski, A. Sobiczewski, Hexadecapole nuclear potential for non-axial shapes. Acta Phys. Pol., B **12**, 1001 (1981). https://doi.org/10.1016/0003-4916(82)90273-1
60. P. Möller, A.J. Sierk, R. Bengtsson et al., Data tables. Atom. Data Nucl. **98**, 149 (2012). https://doi.org/10.1103/PhysRevC.79.064304
61. K. Pomorski, J. Dudek, Nuclear liquid-drop model and surface-curvature effects. Phys. Rev. C **67**, 044316 (2003). https://doi.org/10.1103/PhysRevC.67044316
62. V.M. Strutinsky, Shell effects in nuclear masses and deformation energies. Nucl. Phys. A **95**, 420 (1967). https://doi.org/10.1016/0375-9474(67)90510-6
63. V.M. Strutinsky, 'Shells' in deformed nuclei. Nucl. Phys. A **122**, 1 (1968). https://doi.org/10.1016/0375-9474(68)90699-4
64. S.G. Nilsson, C.F. Tsang, A. Sobiczewski et al., On the nuclear structure and stability of heavy and superheavy elements. Nucl. Phys. A **95**, 1 (1969). https://doi.org/10.1016/0375-9474(69)90809-4
65. Y. Sun, Projection techniques to approach the nuclear many-body problem. Phys. Scr. **91**, 043005 (2016). https://doi.org/10.1088/0031-8949/91/4/043005
66. M. Bender, K. Rutz, P.G. Reinhard et al., Pairing gaps from nuclear mean-field models. Eur. Phys. J. A **8**, 59 (2000). https://doi.org/10.1007/s10050-000-4504-z
67. U. S. National Nuclear Data Center. http://www.nndc.bnl.gov/

Springer Nature or its licensor (e.g. a society or other partner) holds exclusive rights to this article under a publishing agreement with the author(s) or other rightsholder(s); author self-archiving of the accepted manuscript version of this article is solely governed by the terms of such publishing agreement and applicable law.